applied sciences

Article

Experimental Investigation of Controlled and Uncontrolled Rectifiers for Low-Power Wind Turbines

Ahmad Alzahrani

Department of Electrical Engineering, College of Engineering, Najran University, Najran 11001, Saudi Arabia; asalzahrani@nu.edu.sa

Abstract: The holistic objective of producing 100% renewable generated electricity motivates the development of low-power and efficient domestic wind turbines. The wind turbine's efficiency can be maximized by operating it in a variable speed configuration, thus harvesting all the wind power. However, the harvesting process requires a two-stage conversion from AC to DC and from DC–DC or DC–AC. The paper aims to analyze the performance of the first stage of AC–DC rectification in terms of output voltage ripple and voltage regulation when the loading conditions vary abruptly. In addition, this work investigates the basic uncontrolled and controlled rectification methods for low-power wind turbines. The role of the output capacitance and its effect on output voltage ripples is illustrated. Finally, the paper highlights the design of a three-phase controlled rectifier using a simple yet effective firing angle control of a silicon-controlled rectifier (SCR) device. The delay caused due to the firing angle variations is reported in the simulations and experimental results to support the conclusion drawn from this study.

Keywords: wind technologies; low-power wind turbines; rectifiers; single-phase rectifiers; three-phase rectifiers; uncontrolled rectifiers; controlled rectifiers; firing angle control

Citation: Alzahrani, A. Experimental Investigation of Controlled and Uncontrolled Rectifiers for Low-Power Wind Turbines. *Appl. Sci.* **2023**, *13*, 4120. https://doi.org/10.3390/app13074120

Academic Editors: Wei Huang and Eladio Durán Aranda

Received: 14 November 2022
Revised: 7 March 2023
Accepted: 16 March 2023
Published: 23 March 2023

1. Introduction

The alarming state of depleting fossil fuel reserves compels the pursuit of greener energy sources. As a result, wind energy systems (WE systems) are growing at an unprecedented pace [1]. According to the Global Wind Energy Council, in 2019, about 5% of the world's electricity was generated by wind energy systems. This number can reach up to 30% by 2050 [1,2]. Even during the low investment period of the COVID-19 pandemic in 2021, wind energy systems flourished with an annual addition of 94 GW, making the global installed capacity of wind energy systems reach 837 GW [2]. Figure 1 shows the electricity generated in 2021 by wind generators. The investment share of small wind power plants in 2020 is estimated to be more than 6 billion USD, and it is expected to grow by three-fold by 2028 [3]. The WE systems hugely impact carbon emissions, as they curtail 1.2 billion tons of CO_2 annually. Many governments are promoting renewable energy systems with attractive policies in order to achieve net-zero emissions. All these policy initiatives, technological advancements, and cost reductions will enhance new wind energy installations by 110 GW annually until 2026 [2].

The research in the WE systems is a widespread domain, contributing a significant share among renewable generators. As the world's electricity generation aims to come from 100% renewable and clean sources, it will be indispensable to develop reliable WE systems [2,4]. Many technical, financial, and socio-economic reasons make them the most favorable energy source among other renewables. First, it is the most cost-effective method to produce clean electricity in terms of levelized cost. The levelized cost of electricity generated from onshore wind farms is around $30 per megawatt hour or about 2 cents/kW-hr [3,5]. The main reason for the low cost is the recent technological development and friendly policies used to promote renewable energy systems. Secondly, in WE systems, the wind energy rotates the alternator blades to convert the mechanical power into electrical power. The process only utilizes clean, abundantly available, and inexhaustible wind resources, free from emissions [2,4]. As a result, the current-installed capacity of wind energy systems reduces more than 300 million metric tons of greenhouse gases, thus significantly resisting climate change. Moreover, wind turbines can be installed in multi-use sites, for example, agriculture fields, farms, solar parks, islands, or hydel power plants [6].

However, despite all the advantages, many challenges hinder WE systems' growth to their full potential. First, WE systems need strategic locations having abundant winds. These are usually remote inhabited locations without a power grid, so the transmission of wind-generated electricity is a significant problem [6,7]. Improving and expanding the national electricity transmission and dispatch network is a way forward with this problem [6,8]. Wind turbines do not pollute the environment; however, turbine noise is often a concern to some people. Turbine noise can be improved by developing better mechanical and aerodynamic systems, so more research and experiments are needed to overcome this problem [9]. Finally, although WE systems are the cheapest electricity generators among renewable energy systems, technologies such as solar, geothermal, and hydrogen-generated electricity rapidly reduce costs. Thus, the WE systems must continue developing and reducing costs to remain in the competition [6,8,9].

This study highlights the suitable topologies for the rectifier units for small wind energy systems. Both uncontrolled and controlled rectifiers are analyzed in terms of loading effects and voltage ripples. The paper includes analysis, simulation, and experimental results of the half-wave uncontrolled rectifier, full-wave rectifier, and fully controlled SCR device. The effect of increasing or decreasing output capacitance on the output voltage is also discussed concerning small, low-power wind energy systems.

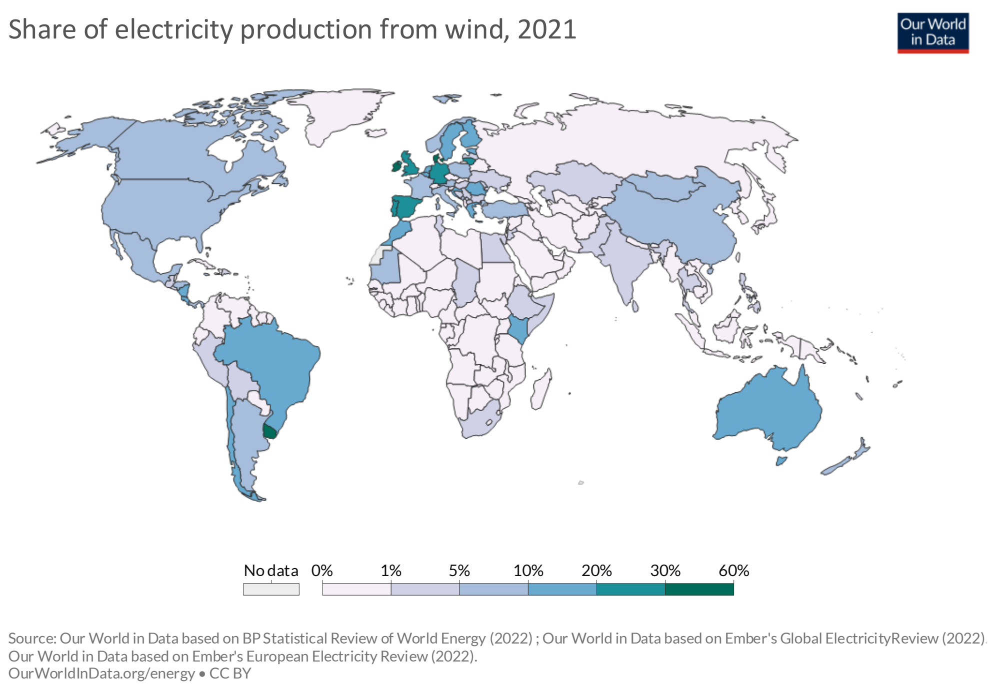

Figure 1. Electricity generated by wind energy in 2021.

2. Overview of Small Wind Turbines

The small-scale WE systems are usually rated under 50 kW and have a hub height of less than 20 m, and offer alternate clean energy to domestic low-power consumers [10]. The small wind energy (SWE) systems couple the mechanical and electrical units. The mechanical unit consists of turbine blades, mechanical assembly, and a gearbox to drive the alternator shaft [11,12]. In comparison, the electrical system consists of a turbine generator, a rectification unit, and a converter or inverter. An electrical generator is the core of wind energy systems. Numerous generator types exist, including permanent magnet synchronous generators, self or separately-excited induction generators, multiple pole generators, and many more [11,13]. In addition, an auxiliary excitation power supply is needed for self/separately excited generators.

The research in modern alternators for WE systems is focused on designing the generators without additional excitation circuits; therefore, multiple-pole permanent magnet synchronous generators are preferred [14]. Further, by reducing or omitting the gearbox assembly, the losses in the mechanical coupling between the rotor and the generator shaft can be significantly reduced. However, the mechanical power at higher wind speeds or at the system's resonance may destabilize the rotor-generator assembly [9,13]. Therefore, feedback control techniques to stabilize the mechanical assembly are often a part of the design process in WE systems [12]. For example, furling control or soft-stall control are renowned techniques to limit the rotational frequency and control the mechanical power of a small wind turbine. Other advanced control techniques include passive blade pitching or electronic feed-back controllers are also popular in high-performance small wind energy systems. In addition, the rotor's efficiency can also be improved with effective yaw control [9,13]. The most straightforward yaw control can be implemented by hinging the tail vane of the rotor's assembly. During high winds, the hinged tail vane rotates the whole assembly, thus reducing the aerodynamic power to remain stable in high winds. However, although the furling technique can achieve power regulation and over-speed protection, the output AC power curve may have some spikes [6]. The power spikes and furling hysteresis may degrade the performance because the wind speed has to drop considerably to unfurl and resume its regular operation. Therefore, an adaptive furling approach is adopted to tackle this problem, where the furling is done electrically in small steps. Additionally, a damper may be required to avoid the chattering when engaging and disengaging the furling action. In contrast to furling, a soft-stall control offers better control in high wins but at a higher cost because an additional DC–DC converter is required between the rectifier and the load [11]. The rectifier and the DC–DC converter are designed to work over a wide range of turbine rpm. Some studies also present hybrid furling and soft-stall control to achieve even better controllability in highly windy conditions [15]. The variable speed wind turbine is coupled to a synchronous/asynchronous generator, followed by a two-stage full power conversion is shown in Figure 2 [8,16].

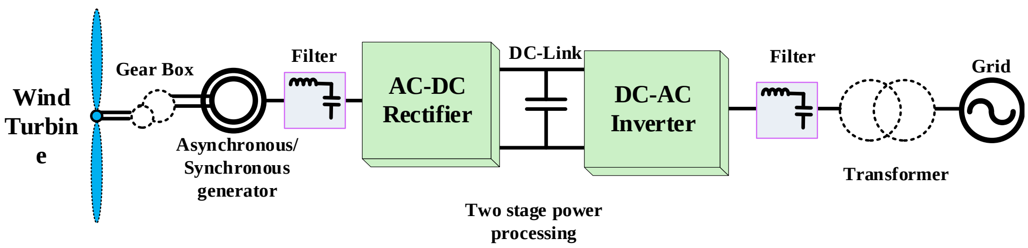

Figure 2. Structure of small wind energy power generation.

The generator unit produces variable AC power proportional to the stochastic wind speed. The rotor speed can be directly measured from the generated AC voltage since the stochastic wind speed produces variable AC amplitude and frequency [7,10]. Therefore, the dynamics of the mechanical parts should be decoupled from the electrical parts. Next, the obtained variable voltage, variable frequency AC, is converted into a DC equivalent to feed a DC load or maintain the DC link voltage for a second-stage converter or inverter. An uncontrolled diode-bridge circuit is the most common rectifier topology for an SWE system [12,13]. The variable AC results in uncontrolled DC, so a unidirectional boost-type DC–DC converter is utilized for DC-link voltage regulation [13]. The DC-link voltage is the input of the second power conversion stage of the WE systems. The second stage is a

DC–DC converter or DC–AC inverter. In contrast, the DC–AC inverter provides the AC power to the AC load or grid [6].

The grid-tied inverters can provide active and reactive power to the power grid [8]. The grid-tied inverter is a complicated device that needs constant grid monitoring; for example, it requires its output voltage to synchronize with the grid voltage simultaneously while injecting active and reactive per-grid codes. The quality of injected power must also comply with specific standards for total harmonic distortion [10]. Furthermore, many parts combine to make the WE systems, and the performance of all parts impacts the overall performance [17]. Therefore, the efficiencies and reliability of both mechanical and electrical systems must be maximized to achieve an optimal SWE system.

3. Rectification Types

The rectification process converts alternating current into a direct current using semiconductors such as diodes and thyristors or silicon-controlled rectifiers (SCRs) [18]. Although there are many topologies for rectifier circuits, the systematic study requires their classification based on some common characteristics. For example, rectification can be classified based on the number of AC phases and controllability [13,19]. The classification of rectifiers is shown in the Figure 3.

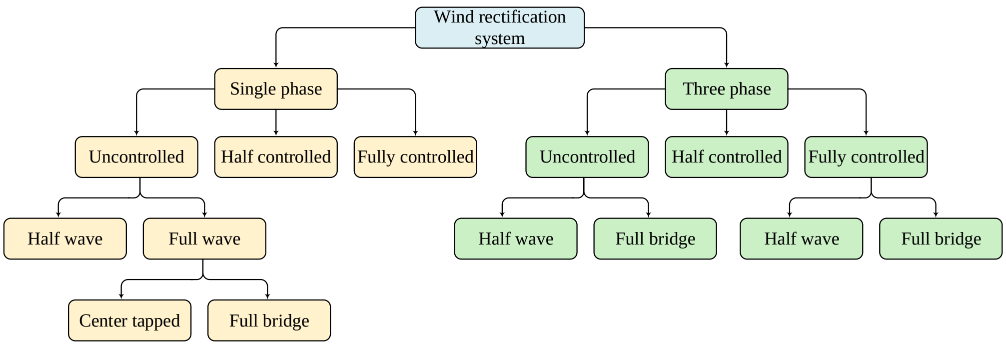

Figure 3. Classification of wind energy systems.

The wind turbine generator can have a single-phase or three-phase output. Single-phase systems are attractive because of their simplicity and reliability. However, three-phase generators are gaining popularity because they are more efficient and have higher power density [20]. The three-phase alternator can extract more power than a single-phase system for the same size. However, a three-phase rectifier needs many more semiconductor devices; therefore, overall losses and system reliability are less compared to a single-phase system. Rectifiers are further differentiated based on controllability [13]. Any rectifier can be uncontrolled, half-controlled, or fully controlled. Uncontrolled rectifiers use only uncontrolled power devices (diodes) to provide a fixed DC output. Uncontrolled rectifiers are the most straightforward and, therefore, the most widely used rectifier circuits [21]. They comprise only an input filter capacitor, semiconductor diodes, and an output filter. Therefore, their output cannot be regulated with varying AC input or because of the load reactance.

3.1. Classification on the Basis of Half or Full AC Wave

When the rectification is performed only for a half-AC cycle, it is said to be a half-wave rectification. Half-wave rectification is a process that allows unidirectional current flow [20]. Half-wave rectification is easily accomplished by basic PN junction diodes, which ensure that during the positive AC cycle, the anode of the PN-junction diode is at a higher voltage potential than the cathode, making the current flow from anode to cathode. On the other hand, during the negative half-cycle, the PN junction's anode is at a lower voltage potential than the cathode, so the diode blocks the negative AC cycle [22].

The rectification is called full-wave rectification if two or more semiconductor switches are connected so that the rectifier circuit makes the bi-directional AC current flow unidirectional for both positive and negative AC [14]. It is evident that full-wave rectification is more efficient, but the efficiency comes with the disadvantage of high cost. The output of the full-wave rectification is also influenced by load reactance and output filtering. The full-wave rectification can be interfaced through two types of input transformers, that is, a center-tapped transformer with two switches, to attain full-wave rectification, and a simple transformer with four switches to attain full-bridge rectification. In addition to the inherent advantage of producing a pulsating DC output in positive and negative AC cycles, the bridge rectifier topology produces almost twice the output voltage compared to the center-tap topology [18]. Therefore, the application of transformers is beneficial, as they can step the AC voltage up or down and provide galvanic isolation to enhance safety. However, transformers also bring additional losses, which may degrade the overall efficiency of the wind energy system.

The ripple factor (RF) is one of the parameters used to benchmark the performance of different types of rectifiers [19]. All the rectifier units convert AC into pulsating DC. Thus, the ratio of the RMS value of the rectified pulsating DC to the average value of pulsating DC is called a ripple factor. The ripple factor is always less than unity, but usually, lower RF indicates smooth and ripple-free output; therefore, a low value of RF is desired [23]. Many studies have reported the theoretical and experimental ripple factors for all the rectifier topologies. For example, the ripple factor of the half-wave rectifier is 1.21, while that of the full-wave rectification is recorded as 0.482. The low-ripple performance can be further improved using three-phase rectifiers.

Peak inverse voltage across the switches of the rectifier circuit indicates reliability [17]. As the number of switches increases, the PIV decreases because the series-connected switches share the peak inverse voltage (PIV). As a result, the half-wave switches face the highest PIV. In contrast, the center tap rectifier configuration PIV is twice that of a bridge rectifier. Therefore, the bridge rectifier configuration suits the application, which has a high DC-link voltage rating.

3.2. Classification on the Basis of Number of Phases

For higher-power wind energy systems, it is recommended to utilize a three-phase rectifier because the phase angle difference between the generated current or voltage phases is 120 degrees [13]. Three-phase rectifiers are composed of three separate current paths. After every 120 degrees, a new phase starts conducting, thus always keeping the output voltage above 86.6% of the maximum voltage, as shown in Figure 4. One of the significant advantages of three-phase full-wave rectifiers is their extraordinarily low ripple factor of 0.17 [18,22]. Moreover, the frequency of the ripples is compared to a half-wave rectifier six times higher, while it is three times higher than the full-wave rectifier. Higher frequency means the output filter components can be less bulky and costly. Along with minimum ripple, the three-phase rectifier has the highest utilization factor. The low ripple factor also increases the life and reliability of the switches and capacitors [17]. However, these advantages come at higher costs and complexity.

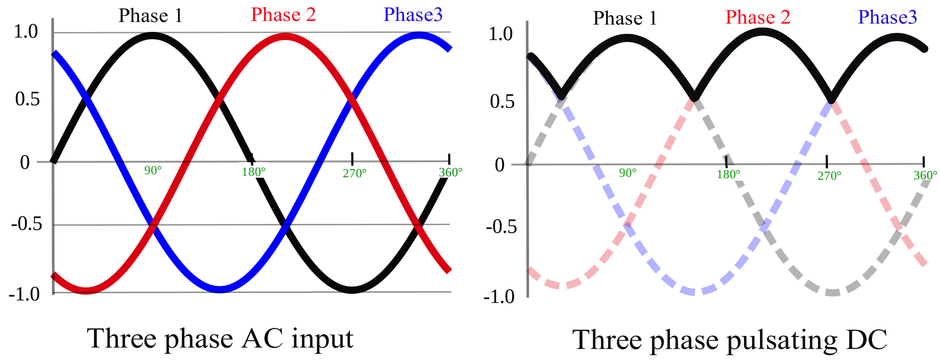

Figure 4. Three−phase half-wave rectification.

3.3. Classification on the Basis of Controllability

All the uncontrollable rectifiers provide constant DC output. However, the wind speed is intermittent; it often increases randomly. Wind energy systems can withstand higher winds, but the output power must be controlled according to the load. The output power of the rectifier can be controlled using a thyristor instead of simple diodes [21]. In addition to anode and cathode terminals, thyristors have an additional control terminal called a gate terminal. Unlike diodes, the thyristor does not conduct by applying a positive voltage across it unless a gate terminal is charged. Thus, the conduction time during the positive AC cycle can be controlled by controlling the firing angle of the thyristor. Once the gate is fired, the thyristor keeps conducting even if the gate signal is removed until the forward current reaches zero [24]. However, in reverse-biased configurations, the thyristor behaves similarly to diodes blocking the voltage until there is a peak inverse voltage. Rectifier circuits are further classified as half-controlled and fully controlled by thyristors. The half-controlled rectifiers consist of both uncontrollable and controllable power devices, that is, diodes and thyristors (SCRs), while the fully controlled rectifier consists of only controllable SCRs to do the rectification. The fully controlled rectifier offers a broader range of control during higher winds compared to half-controlled or uncontrolled rectifiers [25]. However, controlled rectifiers need additional gate control circuitry and sensors to rectify, increasing cost and complexity.

4. Single-Phase Half-Wave Uncontrolled Rectifier

A single-switch half-uncontrolled wave rectifier is the simplest way to convert an AC into a pulsating DC, as shown in Figure 5. During the positive AC cycle, the diode is forward-biased because the diode's anode has a higher voltage potential than the cathode; thus, the input sinusoidal waveform is allowed to pass with a minor voltage drop due to the diode's forward resistance [11]. However, during the negative AC cycle, the diode is reverse-biased because the diode's anode is at a lower voltage potential than the cathode, thus blocking the flow of current to the output. As a result, the output load will experience a pulsating DC.

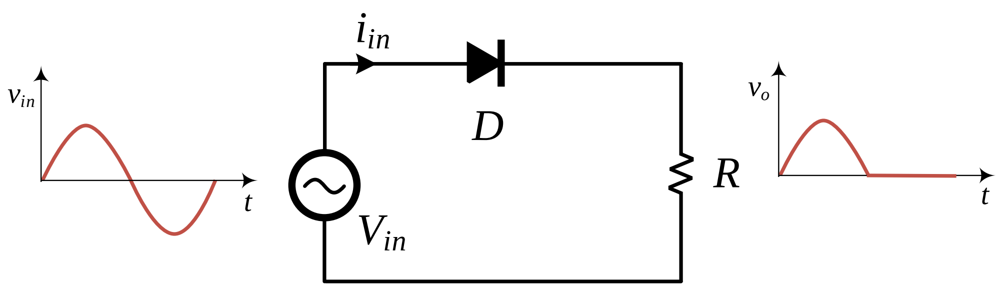

Figure 5. Single-phase half-wave rectification.

The output is always fixed for uncontrolled rectifiers for a given AC supply, but the output ripple, average value, efficiency, and AC harmonics are analyzed to benchmark the rectifier circuits. The AC harmonics are superimposed on the output DC and can be measured in terms of the ripple factor [11]. The ripple factor can be related in Equation (1).

$$RF_v = \frac{V_{ac}}{V_{dc}} = \sqrt{\frac{V_{rms}^2 - V_{dc}^2}{V_{dc}^2}} = \sqrt{\frac{V_{rms}^2}{V_{dc}^2} - 1} = \sqrt{Form\ Factor^2 - 1} = \sqrt{\frac{1}{\eta} - 1} \quad (1)$$

The form factor (FF) is the ratio of the RMS value to the DC average value, and η is the efficiency of the rectifier circuit. The lower ripple factor shows better DC conversion [13]. The average voltage of a single-phase half-wave rectifier can be calculated by integrating the area under the curve of the pulsating output waveform. The average voltage can be expressed as Equation (2).

$$V_{avg} = \frac{1}{T}\int_0^T v(t)dt \quad (2)$$

where T is the time period of a single AC input cycle, and $v(t)$ is the instantaneous value of the voltage. The average voltage can also be calculated by integrating the area under the curve of the current waveform having an instantaneous value of current as $i(t)$. The average current value is depicted in Equation (3) [13].

$$I_{avg} = \frac{1}{T}\int_0^T i(t)dt \quad (3)$$

The RMS voltage and current value can be calculated as in Equations (4) and (5).

$$V_{rms} = \sqrt{\frac{1}{T}\int_0^T v(t)^2 dt} \quad (4)$$

$$I_{rms} = \sqrt{\frac{1}{T}\int_0^T i(t)^2 dt} \quad (5)$$

The output voltage and current significantly depend on the type of load. Ideally, for a purely resistive load, the power factor reaches unity, degrading progressively as the load becomes inductive. For any AC input, the ripple factor and the power factor for a resistive load are 1.21 and 0.707, respectively [20]. The high ripples in the output of the rectifier are undesirable. Connecting capacitive filters in parallel with the load is the most straightforward technique to smooth out the pulsating DC output of the single-phase half-wave rectifier. Since the rectifier is reverse-biased for half the period, a large capacitor is required to support the load for at least half the time period. During the positive AC cycle, the current is supplied to the load, and the capacitor is also charged. When the diode is reverse-biased, the capacitor supplies the power to the load. The output voltage during positive and negative AC cycles can be expressed as a piecewise expression considering a purely resistive load with capacitive filtering, as shown in Equation (6).

$$V_o = \begin{cases} V_m \sin(\omega t) & (Diode\ Forward\ Biased) \\ \sqrt{2}\, V_{in}\ \sin(\theta)e^{-\frac{\omega t - \theta}{\omega RC}} & (Diode\ Reversed\ Biased) \end{cases} \quad (6)$$

where V_o is the output voltage on the load, $\omega = 2\pi f$ is the angular frequency (f = 60 Hz), Vin is the input AC RMS value, R is the resistive load, C is the filter capacitor, and θ is the phase angle between the capacitor voltage V_o and the input voltage V_{in}. The phase angle θ is expressed explicitly as:

$$\theta = \pi - \tan^{-1}(\omega RC) \quad (7)$$

The capacitive filter is charged to 90% of its maximum value according to the charging time constant, which is the product of load (R) times capacitance (C)

$$\tau = RC \tag{8}$$

Observing the relationship between the discharge time, time period, and charging time constant is interesting. As shown in Figure 6a, as the discharge start time decreases, the time constant τ increases, showing an inverse relationship [18]. Similarly, in Figure 6b, the output voltage is directly proportional to the time constant. Since the resistive load is constant, the output voltage can be increased or decreased by increasing or decreasing the capacitance value [26].

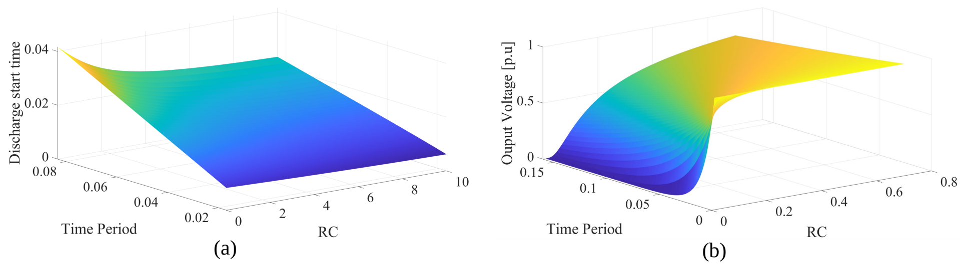

Figure 6. (**a**) Time constant vs. discharge start time; (**b**) time constant vs. output voltage.

This paper reports the effect of the time constant on the discharge start time and the output voltage. The above theoretical analysis is validated by developing a single-phase half-wave hardware prototype. The input AC 208 V_{RMS}/60 Hz supply is stepped down by a transformer having a turn ratio of 7.43. The semiconductor diode 1N007 device rated at 1 A and having a PIV of 1000V is used. A ceramic resistance of 25 Ω is used as a load.

Figure 7a shows the recorded waveforms on the oscilloscope, where channel 1 shows the stepped-down AC sinusoidal voltage measuring 23.45 V_{RMS}. Channel 2 records the peak-to-peak and average current flowing into the load. Since the current is measured through differential probes, the current values are indicated in mV on the oscilloscope trace of channels 2 and 3. In addition, the signals on channels 2 and 3 are amplified by gain 2. Therefore, the calibrated current flow into the load can be calculated from Equation (9).

$$I_{actual} = \frac{I_{Measured}*2}{10*10^{-3}} \tag{9}$$

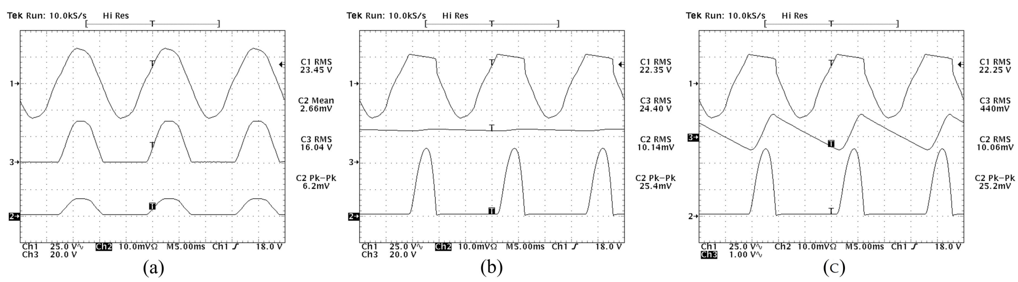

Figure 7. Experimental results of half−wave rectification: (**a**) without output capacitor (**b**) with output capacitor (**c**) the voltage ripples and DC components

The average current measured in Figure 7a (channel 2) is 0.53 A. While Figure 7a channel 3 shows the voltage waveform across the resistive load without a capacitor filter. The half-wave rectifier passes the positive AC cycle to the load and blocks the negative half-cycle, making the voltage RMS value 16.04 V_{RMS}.

Effect of Capacitive Filtering

Capacitors can improve the output ripple performance and can also be used at the input side to smooth out the harmonic and glitches in the source AC supply. A 10 mF capacitor filter was connected in parallel to the load to improve the ripple performance of the half-wave rectifier circuit. At the same time, the same capacitor was also added to the input AC parallel to the transformer-winding, making the sinusoidal input become clamped at a certain voltage. The clamping happens because the diode is forward-biased, and the charging voltage becomes higher than the AC supply voltage [20]. Therefore, the capacitor is charged to a particular value which holds this charge, resulting in a constant clamped input voltage in a positive AC cycle. As a result, the output voltage is smoothed into a constant DC at 24.40 V (Channel 3, Figure 7b) instead of a pulsating DC. The following Table 1 shows the effect of capacitor addition on various parameters of the half-wave rectifier. In Figure 7c, channel 3 shows the DC component of the output voltage. By increasing the capacitance, the output voltage stops pulsating. Thus, the peak-to-peak ripple spans only 440 mV, which is only 2% of the output voltage.

Table 1. Effect of output capacitor on various parameters.

Parameters	Without Capacitor	With Capacitor
RMS Output DC Voltage	23.45 V	22.35 V
RMS Output Voltage Ripple	2000 mV	440 mV
RMS Secondary AC voltage	16.04 V	24.4 V
RMS Secondary Current	-	2.028 A

5. Full-Wave Uncontrolled Rectifiers

Full-wave rectifiers are more efficient than half-wave rectifiers in producing pure DC from an AC power supply. The main advantage of full-wave rectification is that they provide a higher average output voltage with fewer ripples. In full-wave topology, positive and negative AC cycles are made to pass through the load in a positive direction. As a result, the frequency of the obtained pulsating DC is double compared to half-wave rectifiers [20]. There are two standard configurations of full-wave rectifiers, center-tapped and full-bridge. The center-tapped rectifiers have the advantage of using only two diodes, reducing losses. However, a bulky transformer is also needed, increasing the losses and cost [18]. On the other hand, a full-bridge rectification only requires four switches without a transformer, as shown in Figure 8. The average and RMS values of the full-wave bridge rectifier's output voltage are expressed in Equations (10) and (11).

$$V_{o_{avg}} = \frac{V_{in} * \sqrt{2}}{ß} \tag{10}$$

$$V_{o_{RMS}} = \frac{V_{in}}{\sqrt{2}} \tag{11}$$

First, the simulations were performed to verify the operation principles of the full-wave bridge rectifiers. During the first positive AC cycle, the diode D_3 becomes forward-biased, making the current through the load and completing the circuit by making D_2 forward-biased. However, during the negative AC cycle, D_1 and D_4 are forward-biased, thus continuously supplying a pulsating DC to the output load. The voltages across all four diodes are shown in Figure 9a. In contrast, the current flowing across the diodes is shown in Figure 9b. Finally, Figure 9c shows the input and output voltages and currents.

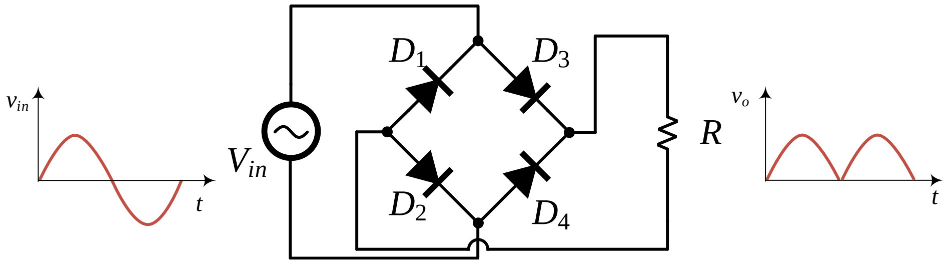

Figure 8. Full-wave bridge rectification.

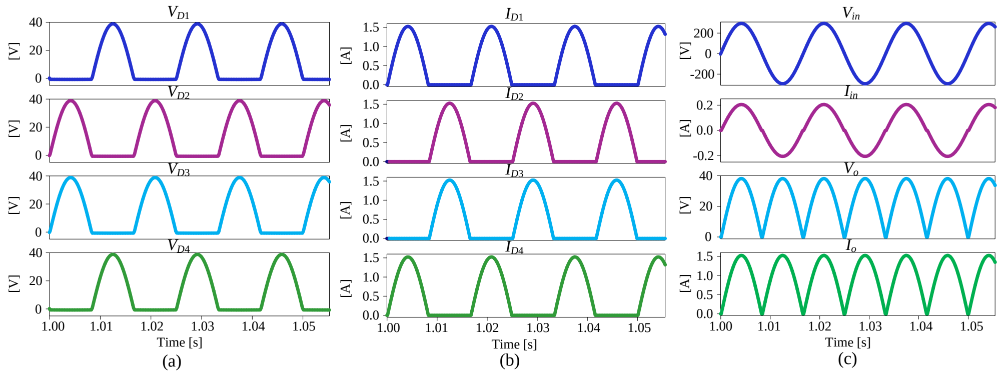

Figure 9. Simulation results of full-wave rectification (**a**) Voltage across the diodes (**b**) currents passing through diodes (**c**) input and output voltages and currents.

The simulation also shows that the ripple frequency was doubled on the output voltage and current compared to half-wave rectifiers. The simulations were validated further by developing a hardware prototype. Table 2 shows the input and output parameters recorded from the experiments. In Figure 10a, channel 1 shows the input AC waveform connected to the bridge rectifier supplying the DC power to the load. The capacitor filter on 10 mF is also connected in parallel to the load, resulting in input sinusoidal wave clamping because the capacitor voltage becomes higher to input AC, and the capacitor holds this charge for both positive and negative AC cycles. Figure 10b shows the AC current measurement at the source before the bridge rectifier. The differential probe measurement shows 7.82 mV, which corresponds to 1.56 A. The output DC voltage at the load is slightly higher than the half-wave rectifier. The oscilloscope trace shows the DC output voltage as 26 V. The output DC voltage is further zoomed in Figure 10b to observe the DC voltage ripples at channel 3. The voltage ripple span is 174 mV, almost two times less than the half-wave rectifier.

Table 2. Measurements for full-wave rectifier.

Parameter	With Capacitor
RMS Output DC Voltage	26.00 V
RMS Output Voltage Ripple	174 mV
RMS Secondary AC voltage	22.5 V
RMS Secondary Current	2.0 A
Amplifier Gain	2

Effect of Load Change

The full-wave bridge rectifier is better in terms of voltage regulation and voltage ripple performance [27]. However, testing the rectifier in varying load conditions is important, especially with an intermittent power source, such as a small wind turbine. The output DC voltage, ripples, and power parameters were observed while increasing and decreasing the load. The load resistance gradually increased from 25 Ω to 250 Ω in four steps. As the load reduced, the output voltage ripple also decreased. However, the relationship between the output voltage ripple and load is non-linear, as shown in Figure 11c. Similarly, the output power and output voltage show an inverse relationship during the unloading experiment, as shown in Figure 11a. At the same time, when the load is gradually reduced, the output voltage ripple and output power show a direct and linear relationship, as shown in Figure 11b. Table 3 shows the observed parameters during the load change experiment. The voltage regulation performance for the full-wave bridge rectifier shows good voltage regulation during the load change experiment. The voltage regulation expression can be calculated as in Equation (12).

Table 3. Parameters during load change experiment.

Load (Ω)	Voltage (V)	Power (W)	Ripple (mV)
25	25.8	26.55	175
75	28.59	10.89	73
137.5	29.55	6.288	45
200	29.98	4.47	33
250	30.2	3.595	29

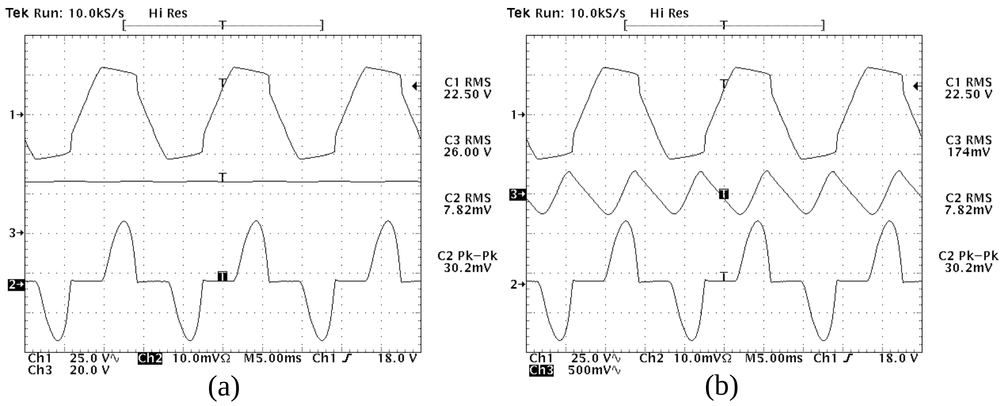

Figure 10. Experimental results of full-wave rectification: (**a**) DC components (**b**) the voltage ripples across the output voltage.

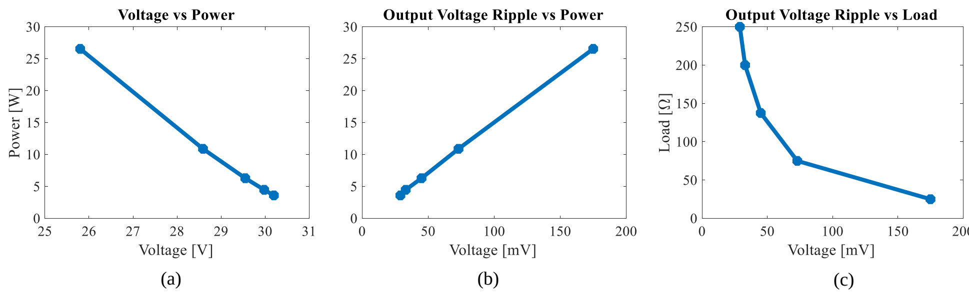

Figure 11. Effect of load change on output voltage regulation: (**a**) voltage vs. Power (**b**) output voltage ripples vs. power (**c**) output voltage ripples vs load.

$$Regulation = \frac{V_{max} - V_{max}}{V_{mid}}\% = \frac{30.2 - 25.8}{29.55}\% = 14.98\% \tag{12}$$

where V_{max} , V_{min} and V_{mid} are the maximum, minimum and mean voltages observed during the experiment.

6. Silicon-Controlled Rectifier

In the previous experiments for single-phase half-wave and full-wave bridge rectifiers, it was established that it is difficult to control the output voltage of the rectifier if the AC source is intermittent, or during varying load conditions. Therefore, a fully controlled bridge rectifier with three semiconductor switches was used to precisely control the output voltage through firing angle control of the switches [21]. Thyristor switches are utilized in this experiment. Thyristors work the same as diodes, except they have an additional gate terminal. Firing a voltage pulse at the gate terminal turns on the thyristors, provided the anode has a higher potential than the cathode. There are many types of three-phase controlled rectifiers. However, a three-phase controlled half-wave rectifier is preferable for small wind-energy systems because of its simplicity, precise output voltage control, high efficiency, and low ripples [20]. The implemented topology is shown in Figure 12.

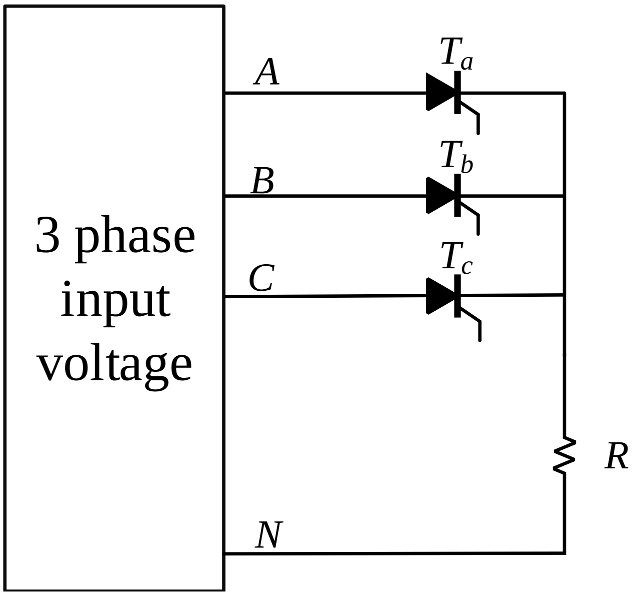

Figure 12. Three-phase half-wave fully controlled rectifier.

The three-phase AC power from a three-phase wind turbine or any other source is connected to the three anodes of the thyristors. Next, the cathodes of the thyristors are shorted to make a common-cathode configuration, and finally, the load is attached. The amplitude of the DC voltage at the load can be controlled by a firing angle delay (α). The theoretical load voltage can be expressed in terms of delay angle α [12], as shown in Equations (13) and (14).

$$V_{dc} = \frac{3\sqrt{3}V_{pk}\cos(\alpha)}{2\pi} \qquad 0 < \alpha < \frac{\pi}{6} \tag{13}$$

$$V_{dc} = \frac{3V_{pk}}{2\pi}\left[1 + \cos\left(\alpha + \frac{\pi}{6}\right)\right] \qquad \frac{\pi}{6} < \alpha < \frac{5\pi}{6} \tag{14}$$

Simulations are performed to verify the theoretical values of Equations (13) and (14). MATLAB SIMULINK with the PLECS toolbox is utilized for the simulations. First, the three-phase AC supply is stepped down using a transformer with the following turns ratio.

$$Turns\ ratio = \frac{N_{primary}}{N_{secondary}} = \frac{208\sqrt{3}}{28} \tag{15}$$

The theoretical, simulation, and experimental values of the output DC voltage for different values of firing angles are shown in Table 4. Data from the experiments show that the delay angle can precisely control the output voltage. As the firing pulse delay increases the output, the DC voltage decreases, as shown in Figure 13.

Table 4. Theoretical simulation and experimental measurements for the three-phase fully controlled rectifier.

Firing Angle	Delay (ms)	Theoretical Voltage	Sim Voltage (V)	Exp Voltage (V)
0	0	32.747	32.66	28.65
15	0.694	31.631	30.75	28.48
30	1.388	28.356	27.91	26.28
45	2.083	23.8	24.239	23.40
60	2.777	19.9066	19.899	20.20
75	3.472	14.013	15.152	16.36
90	4.166	9.4533	10.3259	12.48
105	4.861	5.537	5.814	7.64
120	5.555	2.533	2.674	3.4

The experimental results were collected by building a three-switch fully controlled rectifier. The Figure 14 shows the oscilloscope trace of various waveforms captured during the experiments. Channel 1 shows the stepped-down AC input voltage, channel 2 shows the load current, and channel 3 shows the rectified DC voltage. The pulsating DC voltage results from all three phases rectified and applied to a fixed resistive load. When there is no delay in firing the thyristors (Figure 14a), the rectifier acts as an uncontrolled rectifier and produces pulsating DC of 28.65 VRMS at channel 3. Next, the firing angle is delayed by 15 degrees, and a corresponding DC voltage of 28.28 VRMS appears in channel 3 in Figure 14b. Figure 14c shows that the output DC voltage reduced to 23.40 VRMS with 30 degrees of delay. At the same time, Figure 14d reports its value as 20.20 VRMS when the delay is 45 degrees. The firing angle delay continued to increase by 15 degrees until a maximum delay of 120 degrees was achieved with the reduction in output DC voltage to 3.4 VRMS. This validates the fact that the output voltage of a three-phase rectifier can be controlled by firing angle delay. The results also correspond to the theoretical analysis and simulations.

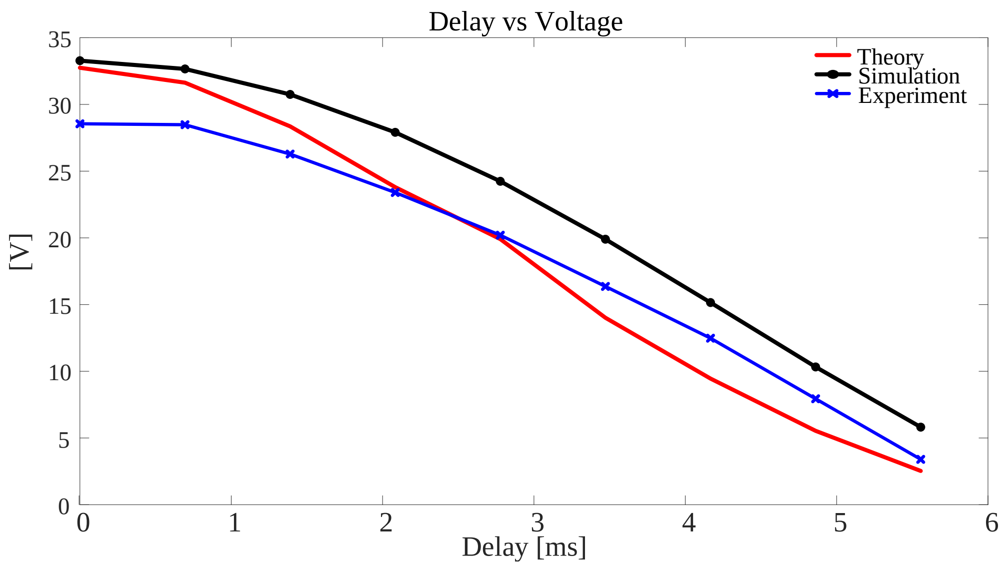

Figure 13. Firing angle delay vs. output voltage.

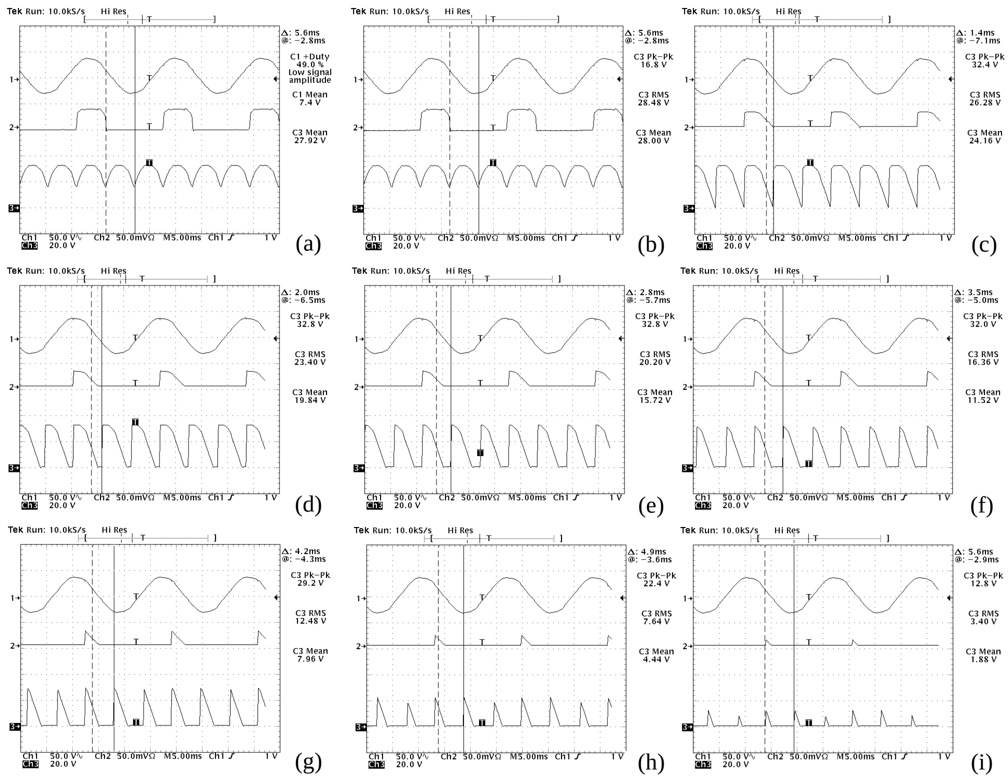

Figure 14. Experimental results for three-phase full-wave rectification: (**a**) firing angle α = 0° (**b**) α = 15° (**c**) α = 30° (**d**) α = 45 (**e**) α = 60° (**f**) α = 75° (**g**) α = 90° (**h**) α = 105° (**i**) α = 120°

7. Experimentation with Small Wind Turbines and Integration of an Inverter

The experiment in this section was performed on a small wind turbine emulator manufactured by Lucas Nuelle. The emulator consists of a battery charge regulator panel, a synchronous generator panel, a three-phase rectifier, a panel with 230 V AC bulbs, an off-grid inverter panel, a variable resistor panel, and a panel for testing the operation of small servo motors.

The emulator uses a synchronous generator with permanent magnets, such as small wind turbines. The generator has a nominal speed of 1000 rpm with 300 W rated power. Generators transform mechanical energy into electricity through electromagnetic induction. Hence, excitation and armature winding speed are critical. An armature winding (usually three-phase) is symmetrically arranged in slots around the generator's stator. The armature induces a voltage when magnetic flux changes. Rotor windings excite, and the excitation winding generates magnetic flux from a direct current. The rotor's mechanical motion rotates the excitation's magnetic field. Even with the current, stator winding conductors create an electromotive force.

The charge controller has been specifically designed for small wind farm installations. It guarantees that the linked battery is fully charged. Suppose the battery cannot be charged anymore. In that case, the load resistor converts the extra energy into heat, which ensures that the motor that serves as the wind generator model is always loaded and prevents it from spinning at excessively high speeds. The panel includes, in addition to the charging regulator, connectors for connecting the wind generator, a rectifier with protection, a protection resistor, a battery, and a connection for external loads. The rectifier converts the three-phase input voltage to a DC voltage. Figure 15 shows the experimental setup of the wind turbine system and the output waveforms. The wind generator was controlled to power a 25 W incandescent lamp. The power from the wind generator is first rectified and controlled with the charge controller, and then the power is inverted from DC to AC through a 230 V, 50 Hz inverter. The sample of output waveforms at each stage is shown in Figure 15.

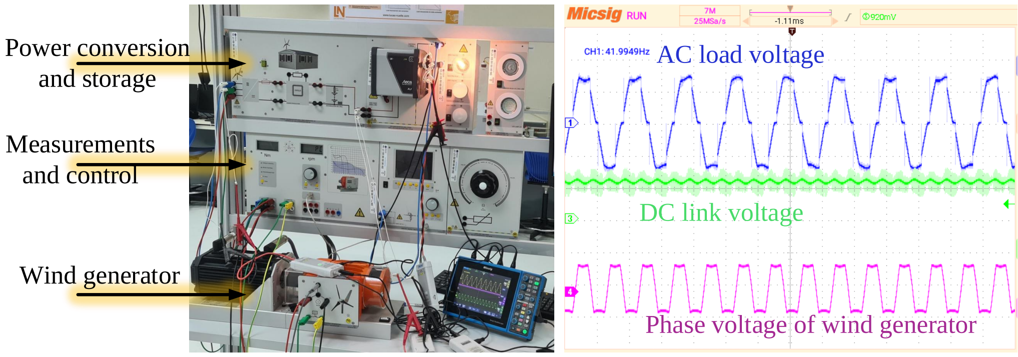

Figure 15. Experimental results for three-phase full−wave rectification used in small wind turbine application.

8. Conclusions

Low-power wind energy systems are proliferating rapidly, so improving and optimizing their mechanical and electrical parts is pivotal. First, the paper provided a valuable review of low-power wind energy systems and their rectifier circuits. Next, various AC to DC rectifier topologies suited for low-power wind energy systems were discussed. Next, the single-phase half-wave rectifier was studied regarding output voltage ripple performance. The rectifier was mathematically analyzed, followed by simulations and experiments. It was found that the filtering capacitor must be large enough to supply DC power to the load during the negative half-cycle. The filtering capacitor improves both the output voltage regulation and voltage ripple performance. The relationship between the charging time constant and the output voltage was also validated for single-phase half-wave rectifiers. Next, the single-phase bridge rectifier was studied in terms of voltage ripples and voltage regulation. The output voltage remains regulated and ripple-free for a reasonable range of the load change (25–250 Ω). Finally, the fully controlled three-phase rectifiers were implemented. The output voltage was controlled through a firing angle delay. The simulations and the experiment showed that the output DC voltage can be regulated through SCR firing angle control at the desired value during wind speed variation and load change.

Funding: This work was funded by the Research Groups Funding program grant code (NU/RG/SERC/11/2).

Institutional Review Board Statement: Not applicable.

Informed Consent Statement: Not applicable.

Data Availability Statement: Not applicable.

Acknowledgments: The author is thankful to the Deanship of Scientific Research at Najran University for funding this work under the Research Groups Funding program grant code (NU/RG/SERC/11/2).

Conflicts of Interest: The author declares no conflict of interest.

Abbreviations

The following abbreviations are used in this manuscript:

SCR	Silicon Controlled Rectifier
PIV	Peak inverse voltage
WE	Wind Energy
RF	Ripple Factor
RMS	Root Mean Square
SWE	Small Wind Energy

References

1. Jones, D.; Graham, E.; Tunbridge, P.; Ilas, A. Global Electricity Review. 2020. Available online: https://ember-climate.org/wp-content/uploads/2020/03/Ember-2020GlobalElectricityReview-Web.pdf (accessed on 1 October 2022).
2. WMO. *State of the Global Climate 2021*; WMO: Geneva, Switzerland, 2022.
3. US Department of Energy. *Levelized Costs of New Generation Resources in the Annual Energy Outlook 2022*; US Department of Energy: Washington, DC, USA, 2022.
4. Rave, K.; Teske, S.; Sawyer, S. *Global Wind Energy Outlook 2014*; Global Wind Energy Council: Brussels, Belgium, 2014.
5. Orrell, A.C.; Sheridan, L.M.; Kazimierczuk, K. *Distributed Wind Market Report: 2022 Edition*; Technical Report; Pacific Northwest National Lab (PNNL): Richland, WA, USA, 2022.
6. Kashem, S.B.A.; Chowdhury, M.E.; Khandakar, A.; Ahmed, J.; Ashraf, A.; Shabrin, N. Wind power integration with smart grid and storage system: Prospects and limitations. *Int. J. Adv. Comput. Sci. Appls.* **2020**, *11*, 5. [CrossRef]
7. Biernatzki, R.; Bechthold, J.; Stauss, W. Small wind turbines applied to rural areas for independent power supply. In Proceedings of the 2012 47th International Universities Power Engineering Conference (UPEC), Middlesex, UK, 4–7 September 2012; pp. 1–4.
8. Joshi, S.; Karamta, M.; Pandya, B. Small scale wind & solar photovoltaic energy conversion system for DC microgrid applications. *Mater. Today Proc.* **2022** , *62*, 7092–7097.
9. Lujano-Rojas, J.M.; Dufo-López, R.; Bernal-Agustín, J.L. Optimal sizing of small wind/battery systems considering the DC bus voltage stability effect on energy capture, wind speed variability, and load uncertainty. *Appl. Energy* **2012**, *93*, 404–412. [CrossRef]
10. Salgado, V.; Troya, C.; Moreno, G.; Molina, J. Airfoil selection methodology for small wind turbines. *Int. J. Renew. Energy Res.* **2016**, *6*, 1410–1415.
11. Kumari, A.; Mahto, C.B.; Padhee, S. Topology and Control Scheme of Machine Side Converter for Wind Power Conversion System. In Proceedings of the 2022 IEEE 2nd International Conference on Sustainable Energy and Future Electric Transportation (SeFeT), Hyderabad, India, 4–6 August 2022; pp. 1–6.
12. Peng, X.; Liu, Z.; Jiang, D. A review of multiphase energy conversion in wind power generation. *Renew. Sustain. Energy Rev.* **2021**, *147*, 111172. [CrossRef]
13. Vilathgamuwa, D.M.; Jayasinghe, S.G. Rectifier systems for variable speed wind generation-a review. In Proceedings of the 2012 IEEE International Symposium on Industrial Electronics, Hangzhou, China, 28–31 May 2012; pp. 1058–1065.
14. Chub, A.; Husev, O.; Blinov, A.; Vinnikov, D. Novel isolated power conditioning unit for micro wind turbine applications. *IEEE Trans. Ind. Electron.* **2016**, *64*, 5984–5993. [CrossRef]
15. Zouheyr, D.; Baghli, L.; Abdelmadjid, B. Real-Time Emulation of a Grid-Connected Wind Energy Conversion System Based Double Fed Induction Generator Configuration under Random Operating Modes. *Eur. J. Electr. Eng.* **2021**, *23*, 207–219. [CrossRef]
16. Labuschagne, C.J.; Kamper, M.J. Wind generator impedance matching in small-scale passive wind energy systems. *IEEE Access* **2021**, *9*, 22558–22568. [CrossRef]
17. Fischer, K.; Pelka, K.; Bartschat, A.; Tegtmeier, B.; Coronado, D.; Broer, C.; Wenske, J. Reliability of power converters in wind turbines: Exploratory analysis of failure and operating data from a worldwide turbine fleet. *IEEE Trans. Power Electron.* **2018**, *34*, 6332–6344. [CrossRef]
18. Gomez-Casseres, E.A.; Arbulú, S.M.; Franco, R.J.; Contreras, R.; Martínez, J. Comparison of passive rectifier circuits for energy harvesting applications. In Proceedings of the 2016 IEEE Canadian Conference on Electrical and Computer Engineering (CCECE), Vancouver, BC, Canada, 15–18 May 2016; pp. 1–6.
19. Haider, S.; Mansor, H.; Khan, S.; Arshad, A.; Shobaki, M.M.; Tasnim, R. A Comparative Study of Small Voltage Rectification Circuits for Implanted Devices. In Proceedings of the IOP Conference Series: Materials Science and Engineering, Kuala Lumpur, Malaysia, 2–4 July 2013, Volume 53, p. 012024.
20. Joshi, M.V. Comparison of rectification topologies with Matlab/Simulink model simulations. In Proceedings of the 2014 International Conference on Circuits, Power and Computing Technologies [ICCPCT-2014], Nagercoil, India, 20–21 March 2014; pp. 1038–1042.
21. Gelman, V. Thyristor Controlled Rectifiers (TCR) for traction-problems and solutions. In Proceedings of the 2013 3rd International Conference on Electric Power and Energy Conversion Systems, Istanbul, Turkey, 2–4 October 2013; pp. 1–6.
22. Buticchi, G.; Lorenzani, E.; Immovilli, F.; Bianchini, C. Active rectifier with integrated system control for microwind power systems. *IEEE Trans. Sustain. Energy* **2014**, *6*, 60–69. [CrossRef]
23. McVey, E.; Russell, R. The design of a simple single phase silicon controlled rectifier regulator. *IEEE Trans. Ind. Electron. Control. Instrum.* **1967** , 8–14. [CrossRef]
24. Nøland, J.K.; Hjelmervik, K.B.; Lundin, U. Comparison of thyristor-controlled rectification topologies for a six-phase rotating brushless permanent magnet exciter. *IEEE Trans. Energy Convers.* **2015**, *31*, 314–322. [CrossRef]
25. He, J.; Wang, Y.; Hu, Y.; Yu, D.; Wang, Y. Improvement of failure current in modified later silicon-controlled rectifier device with N-type floating region. In Proceedings of the 2020 IEEE 15th International Conference on Solid-State & Integrated Circuit Technology (ICSICT), Kunming, China, 3–6 November 2020; pp. 1–3.

26. Dahbi, A.; Nait-Said, N.; Hamouda, M.; Arama, F.Z. Analysis of different converters used in wind energy conversion system. In Proceedings of the 2014 International Renewable and Sustainable Energy Conference (IRSEC), Ouarzazate, Morocco, 17–19 October 2014; pp. 352–359.
27. Daoud, M.; Elserougi, A.; Massoud, A.; Bojoi, R.; Ahmed, S. Series-Connected Multi-Half-Bridge Modules Active Front-End Rectifier for Medium Voltage Variable Speed Drives. In Proceedings of the 2018 21st International Conference on Electrical Machines and Systems (ICEMS), Jeju, Korea, 7–10 October 2018; pp. 2436–2440.